Dimerization and Folding of LC8, a Highly Conserved Light Chain of Cytoplasmic Dynein†

Elisar Barbar,*,‡ Brian Kleinman,‡ Daniel Imhoff,‡ Mingang Li,§ Thomas S. Hays,§ and Michael Hare‡

Department of Chemistry and Biochemistry, Ohio University, Athens, Ohio 45701, and Department of Genetics, Cell, and Developmental Biology, University of Minnesota, Minneapolis, Minnesota 55455

Received September 28, 2000; Revised Manuscript Received November 28, 2000

ABSTRACT: Cytoplasmic dynein is a multisubunit ATPase that transforms chemical energy into motion along microtubules. LC8, a 10 kDa light chain subunit of the dynein complex, is highly conserved with 94% sequence identity between *Drosophila* and human. The precise function of this protein is unknown, but its ubiquitous expression and conservation suggest a critical role in the function of the dynein motor complex. We have overexpressed LC8 from *Drosophila melanogaster* and characterized its dimerization and folding using analytical ultracentrifugation, size-exclusion chromatography, circular dichroism, and fluorescence spectroscopy. Sedimentation equilibrium measurements of LC8 at pH 7 reveal a reversible monomer−dimer equilibrium with a dissociation constant of 12 μM at 4 °C. At lower pH, LC8 dissociates to a monomer, with a transition midpoint at pH 4.8. Far-UV CD and fluorescence spectra demonstrate that pH-dissociated LC8 retains native secondary and tertiary structures, while the diminished near-UV CD signal shows loss of quaternary structure. The observation that dimeric LC8 dissociates at low pH can be explained by titration of a histidine pair in the dimer interface. Equilibrium denaturation experiments with a protein concentration range spanning almost 2 orders of magnitude indicate that unfolding of LC8 dimer is a two-stage process, in which global unfolding is preceded by dissociation to a folded monomer. The nativelike tertiary structure of the monomer suggests a role for the monomer−dimer equilibrium of LC8 in dynein function.

Cytoplasmic dynein is a principal motor for minus end-directed intracellular transport along microtubules. It functions in mitotic spindle assembly, in positioning of the Golgi complex, and in the transport of other membranous organelles (*1*, *2*). Cytoplasmic dynein is a 1.2 MDa multisubunit protein complex composed of a homodimer of heavy chains (∼530 kDa) and two to three intermediate chains (∼74 kDa), as well as several light intermediate (52−61 kDa) and light chains (10−25 kDa). As viewed by electron microscopy, the heavy chains form two globular heads joined by flexible stalk domains to a common base. The heavy chains contain the microtubule binding sites and the hydrolytic ATP binding sites required for force production. The set of lower molecular weight subunits located at the base of the motor complex are thought to participate in complex assembly and the coupling of the dynein motor to a variety of cellular cargo (*3*, *4*).

All known cytoplasmic and axonemal dyneins contain LC8, a 10 kDa dynein light chain with a highly conserved sequence among species (*5*−*9*; and Li and Hays, unpublished data). Molecular genetic studies in several organisms including *Drosophila*, *Chlamydomonas*, and *Aspergilus* show the functional significance of this subunit. For example, hypomorphic mutations in a *Drosophila* LC8 gene result in defects in oogenesis and female sterility, as well as defects in neuronal pathfinding during later stages of embryogenesis (*6*, *10*). Furthermore, null mutations in *Drosophila* LC8 are lethal, demonstrating that it has one or more essential functions. In *Aspergilus*, mutations in the LC8 homologue, NudG,[1] give rise to defects in nuclear migration and positioning. LC8 mutants in *Chlamydomonas* are defective in flagellar motility and retrograde intraflagellar transport (*11*).

Two roles have been proposed for the LC8 subunit in dynein function. First, LC8 may promote the assembly of the dynein motor complex. Dissociation of rat cytoplasmic dynein results in an intermediate complex containing LC8, LC14 (a 14 kDa light chain), and IC74, (a 74 kDa intermediate chain) (*12*). The LC8 subunit is also present in myosin V and may serve a similar function in the assembly of its dimeric heavy chain motor subunits (*13*). Second, LC8 may be involved in targeting the complex to specific cargoes, as suggested by recent reports of interactions with a number of unrelated cellular proteins. For example, human or rat LC8

† This work is supported by grants from Ohio Cancer Research Associates (E.B.), by NIH Grants GM60969 (E.B.) and GM44757 (T.S.H.), by an American Heart Established Investigator Award (T.S.H.), and by the American Cancer Society (M.H.).

* Correspondence should be addressed to this author at the Department of Chemistry and Biochemistry, Ohio University, Athens, OH 45701. Tel: (740) 593-1751. Fax: (740) 593-0148. E-mail: barbar@ohio.edu.

‡ Ohio University.

§ University of Minnesota.

[1] Abbreviations: CD, circular dichroism; HPLC, high-performance liquid chromatography; SEC, size-exclusion chromatography; PIN, LC8 from rat or human, protein inhibitor of neuronal nitric oxide synthase (nNOS); NudG, LC8 from *Aspergilus nidulans*; DTT, dithiothreitol; TCEP, tris(2-carboxyethyl)phosphine; GdnCl, guanidine hydrochloride.

10.1021/bi002278+ CCC: $20.00 © 2001 American Chemical Society
Published on Web 01/17/2001

(called PIN) is proposed to interact with and inhibit neuronal nitric oxide synthase (nNOS) activity (*14*), or to facilitate the transport of nNOS along the microtubules within axons (*15*). In vertebrates, LC8 is reported to interact with IκBα, a key molecular target involved in transcriptional regulation of NF-κB during viral infection or inflammatory reactions (*16*), and with bim, a small protein of the Bcl2 family which is suggested to regulate proapoptotic activity (*17*). In *Drosophila*, LC8 is reported to interact with Swa, a protein that co-localizes with bicoid RNA during oogenesis, and may act as an adapter to enable dynein to transport RNA along microtubules (*18*). Direct attachment of LC8 to the 3′-untranslated region of parathyroid hormone mRNA, and co-localization of LC8 and this mRNA to microtubules, has been reported (*19*).

To begin to address the mechanistic basis of LC8 function, our investigations are directed toward understanding the relationship between the tertiary and quaternary structure of LC8 and its interactions with biologically relevant macromolecules. Here we are interested in the quaternary interactions governing LC8 self-association. The presence of two copies of LC8 within the cytoplasmic dynein complex suggests that dimerization of this subunit may be important for assembly and function of the motor complex (*20*). The recently published crystal structure of PIN (human LC8) homodimer bound to two identical peptide fragments of nNOS shows that binding of the peptides occurs very close to the dimer interface. Since each peptide interacts to some extent with both subunits of the dimer, it may be inferred that dimerization strengthens the PIN−peptide interaction (*21*).

In this work, we employ a variety of biophysical techniques to characterize the self-association and folding of *Drosophila* LC8 dimer and to identify conditions for shifting the monomer−dimer equilibrium. We have also characterized the self-association of LC8 from *Aspergilus nidulans*, NudG. Previous investigations of the association state of the LC8 homologue PIN have reached divergent conclusions (*15, 22, 23*). By comparison of the primary structure and other properties of these LC8 variants (NudG, PIN, and *Drosophila* LC8), and examination of the crystal structure of PIN (*21*), we identify residues at the dimer interface which contribute to dimer stability. This investigation into the biophysics of LC8 self-association is a step toward understanding the mechanism and forces that contribute to assembly and function of LC8 in the dynein complex.

MATERIALS AND METHODS

Stock Solutions and Buffers. Since *Drosophila* LC8 contains two free thiol groups, Cys 24 and Cys 56, all data were obtained on samples in 5−10 mM TCEP or DTT to rule out the possible contribution of intermolecular disulfide bonds to self-association. PBS buffer is used in analytical ultracentrifugation with 10 mM TCEP. Buffers for pH dependence were all 10 mM acetate for pH lower than 5, 10 mM phosphate for pH 6−7, and 10 mM Tris for pH 8.5. All buffers contained 0.1 M NaCl, unless otherwise indicated. Samples for CD and fluorescence measurements at pH 3 were in 10 mM glycine, 0.1 M NaCl, 5 mM TCEP. Glycine buffer was prepared by diluting 0.2 M glycine hydrochloride and adjusting to the appropriate pH. TCEP stock solutions were prepared in the appropriate buffer and adjusted with NaOH to the required pH. Samples for CD and fluorescence measurements at pH 7 were in 10 mM sodium phosphate, 0.1 M NaCl, and 5 mM TCEP. Solutions of 8 M GdnCl were prepared as described elsewhere (*24*), and the exact concentration was determined by refractive index. All buffers and GdnCl solutions were freshly prepared and filtered through a 0.22 μm filter prior to use. LC8 stock solutions were dialyzed in the appropriate buffers and their concentrations determined from the absorbance at 280 nm using a molecular weight of 10 373.6 and an extinction coefficient of 1.39 mg^{-1} cm^{-1} mL. The extinction coefficient was calculated from the number of Trp and Tyr residues (*25*).

Expression and Protein Purification. The gene encoding the 10 kDa *Drosophila* dynein light chain was subcloned into the bacterial expression vector pTrcHis which has an N-terminal hexa-His tag (Invitrogen), and transformed in the *E. coli* DH5α cell line. A protease factor Xa recognition sequence was engineered immediately 5′ to the start codon of the LC8 cDNA clone. Cells were grown to an OD_{600} of 0.6, and expressed protein was induced with isopropyl-β-D-thiogalactoside (IPTG) to a final concentration of 0.4 mM at 27 °C for 8−12 h. The cell pellet was resuspended in 20 mM phosphate buffer, pH 7.8, containing 0.5 M NaCl, 5 mM β-mercaptoethanol, 100 μg/mL lysozyme, and 1 mM phenylmethylsulfonyl fluoride (PMSF) and incubated on ice for 15 min. After sonication and centrifugation, the crude extract was purified by affinity chromatography on Ni−NTA (nitrilotriacetic acid) resin (Qiagen Inc.) by elution with 350 mM imidazole at pH 6. The fusion protein was dialyzed against 20 mM Tris buffer, pH 8.0, containing 0.2 M NaCl and 2 mM $CaCl_2$ and incubated with 1% factor Xa (New England BioLabs) for 9 h at 37 °C. Completion of the reaction was monitored by SDS−PAGE. Cleavage of the His tag by factor Xa releases the native sequence of LC8. The protein was further purified from the fusion peptide and the protease on a High Q DEAE anion-exchange resin (Bio-Rad) and eluted with 0.1 M NaCl. The free thiol content of the protein was estimated using Ellman's reagent, 5,5′-dithiobis(2-nitrobenzoic acid) (DTNB) (*26*). Purity was determined by analytical SEC and SDS−PAGE to be >98%. The mass obtained from electrospray ionization mass spectrometry (ESMS) was 10 373 ± 1.0 amu (calculated mass 10 373.6 Da).

For purposes of comparison, LC8 from *Aspergilus* (NudG) was also produced. The *E. coli* vector pGEX-KG (*27*) containing the NudG gene, a GST-tag, and a thrombin cutting site (kindly provided by Dr. B. Liu, University of California, Davis) was transformed into BL21 cell lines (Amersham Pharmacia Biotech). Cells were grown to an OD_{600} of 1, and protein expression was induced with 0.1 mM IPTG at 27 °C for 12 h. Pellets were resuspended in PBS buffer containing 2 mM EDTA, 10 mM β-mercaptoethanol, 2 mM PMSF, 5 mM benzamidine, and 1% Triton X. The crude extract was purified on a glutathione Sepharose affinity column (Amersham Pharmacia Biotech). The fusion protein was eluted with glutathione elution buffer (10 mM reduced glutathione, 50 mM Tris-HCl, pH 8) and incubated with thrombin protease (10 μL/mg of protein) for 16 h at 25 °C. Completion of the cleavage reaction was monitored on SDS−

PAGE. LC8 was purified from the fusion protein on a 600 mm Superdex 75 size-exclusion column (Amersham Pharmacia Biotech), and the purity was determined by analytical SEC and SDS−PAGE. The mass obtained from ESMS was 12 116 ± 1.7 amu, in good agreement with the expected mass.

Analytical Ultracentrifugation. Sedimentation velocity and equilibrium experiments were conducted using a Beckman Optima XL-A analytical ultracentrifuge following published procedures (*28*). For sedimentation velocity, a rotor speed of 60 000 rpm was used for three protein concentrations. For sedimentation equilibrium experiments, three loading concentrations (19, 58, 174 μM) were sedimented to equilibrium at three speeds (25 000, 29 000, and 43 000 rpm) and scanned at 280 nm using cell path lengths of 3 or 12 mm. Samples were allowed to equilibrate for 16 h at each speed and concentration, and were considered at equilibrium when sequential scans 2 h apart were superimposable. Data were acquired as averages of 25 measurements of absorbance at each radial position, with a nominal spacing of 0.001 cm between each position. The data of three speeds and three concentrations were globally fit to a monomer−dimer self-association model, and resulted in random residuals (Figure 1 and Table 1). Other models were tried but did not give adequate variances and random residuals. All experiments were done at 4 °C.

Size-Exclusion Chromatography−HPLC. The association state of LC8 was determined by comparing elution times to a set of molecular weight standards on a TSK2000SW (TosoHaas) size-exclusion HPLC column (7.8 mm × 60 cm, particle size 5 μm, flow rate 1 mL/min). Proteins were detected by the absorbance at 280 and 230 nm. The running buffer was 0.1 M sodium citrate/phosphate, 0.3 M sodium sulfate, 5 mM DTT, and 1 mM sodium azide. A mixture of citrate and phosphate was used to allow for spanning a pH range from 2 to 8 while changing only the ratio of citrate to phosphate. Before loading, LC8 samples were equilibrated at room temperature for at least 48 h, and the column was equilibrated at the appropriate pH for 1 h.

Circular Dichroism and Fluorescence Measurements. CD experiments were conducted on a JASCO 715 spectropolarimeter equipped with a Peltier type cell holder (model PFD-335S) which permits accurate temperature control. A built-in magnetic stirrer allows for fast equilibration within the cell. For thermal denaturation experiments, protein samples were prepared at pH 4, at a concentration of 3 μM, in 2 mM TCEP, and recorded in the far-UV CD using a 1 cm cell. Low protein concentration is used to prevent aggregation at high temperature. The temperature was lowered periodically during the runs to minimize irreversible denaturation by prolonged heating. Reversibility of ~90% was determined by comparison of measurements taken at low temperature before and after the experiment.

For GdnCl unfolding, experiments were recorded in a 1 or 2 mm cell for far-UV CD data, and in a 1 cm cell for near-UV data. Data were collected at 30 °C using a batch-type experiment to ensure that equilibrium was achieved. Samples were equilibrated for 18 h at room temperature and incubated at 30 °C in a water bath for 1 h prior to acquisition. Spectra were corrected by subtraction of a blank acquired for each sample. The association states of protein samples used for thermal and chemical denaturation were verified to be monomeric or dimeric by size-exclusion chromatography. Reversibility was determined after dialysis in native buffer.

Intrinsic fluorescence emission spectra of the single tryptophan were acquired on a Jobin Yvon/Spex spectrofluorometer. The excitation wavelength was set to 281.5 nm, and fluorescence emission spectra were scanned from 300 to 380 nm, with excitation and emission bandwidths adjusted depending on the protein concentration used. To limit the impact of photobleaching at low protein concentrations, samples were stirred continuously, and only one measurement per sample was recorded. The conditions (protein concentrations, buffer, and temperature) of the unfolding experiments were the same as those for CD. All experiments were carried out at 30 °C, using an external circulating bath.

Analysis of Equilibrium Denaturation Data. Chemical denaturation of LC8 at pH 7 and greater than 0.5 μM protein concentration results in two distinct transitions (see Figure 7). We have analyzed our data using the model described by eq 1, where a second-order (concentration-dependent) dissociation is followed by first-order unfolding. To account for the change in reaction order, the first and second transitions were modeled separately. The fitted lines in Figures 4, 6, and 7 are a normalized summation of the results of the two models.

$$\mathrm{D} \overset{K_d}{\rightleftharpoons} 2\mathrm{M} \overset{K_u}{\rightleftharpoons} 2\mathrm{U} \tag{1}$$

The free energy changes of both transitions, $\Delta G_{H_2O,1}$ and $\Delta G_{H_2O,2}$, were determined by a fit of the free energy ΔG_i (calculated as $\Delta G = -RT \ln K$) for points in the transition regions of each denaturation curve using eq 2. In eq 2, [GdnCl] is the concentration of denaturant, and m is the slope of the line given by a plot of ΔG_i vs [GdnCl]; ΔG_{H_2O} is the intercept of the line, which gives the free energy of denaturation or unfolding at 0 M GdnCl (*24, 29−31*).

$$\Delta G_{H_2O} = m[\mathrm{GdnCl}] + \Delta G_i \tag{2}$$

K_d for the first transition was determined using eq 3, where P_t is the concentration of protein and f_m is the fraction of monomer (*32*). The fraction of monomer is related to experimental parameters by eq 4, where y_d is the spectrometric signal associated with pure dimer, y_m is the signal of pure monomer, and y_i is the signal at some concentration of denaturant. The midpoint of the dissociation transition, $C_{m,1}$, was calculated using eq 5.

$$K_d = \frac{[\mathrm{M}]^2}{[\mathrm{D}]} = \frac{2P_t f_m^{\,2}}{1 - f_m} \tag{3}$$

$$f_m = \frac{y_d - y_i}{y_d - y_m} \tag{4}$$

$$C_{m,1} = [-RT \ln(P_t) + \Delta G_{H_2O,1}]/m_1 \tag{5}$$

The free energy of the second transition was calculated in a similar manner, but using eq 6 to define the first-order equilibrium constant, and eq 7 for the relation of the fraction of unfolded protein, f_u, to the signal of unfolded protein, y_u, and other spectroscopic parameters. The midpoint of the unfolding process, $C_{m,2}$, was determined using eq 8.

$$K_u = \frac{[U]}{[M]} = \frac{f_u}{1 - f_u} \quad (6)$$

$$f_u = \frac{y_m - y}{y_m - y_u} \quad (7)$$

$$C_{m,2} = \Delta G_{H_2O,2}/m_2 \quad (8)$$

In practice, free energies and other characteristic features of the denaturation curves were determined by fitting the calculated spectroscopic signal to the experimentally determined signal. $\Delta G_{H_2O,1}$ and $\Delta G_{H_2O,2}$ were globally fit to a data set which included each denaturation curve at a given pH and temperature. Parameters of the fit which were optimized for individual curves were y_d, y_m, y_u, m_1, and m_2. Where the dissociation transition was not evident, such as denaturation at pH 3 or when the effect of added denaturant was monitored by far-UV CD, only the parameters relevant to unfolding were optimized, and the results were normalized to 0.5 to make them consistent with the presentation of other data. The fits were performed using a χ^2 procedure implemented in Microsoft Excel.

RESULTS

Size-Exclusion Chromatography. Size-exclusion chromatography indicates that the ratio of dimer to monomer increases as a function of both protein concentration and pH (data not shown). At pH 7, a single peak with a retention time corresponding to dimeric LC8 is observed. No soluble higher aggregates are detected at protein concentrations up to 390 μM. At pH 4.5, there is a peak with a retention time corresponding to LC8 monomer in addition to the dimer peak. The presence of two peaks indicates that the monomer−dimer equilibrium is slow relative to the analysis time (12−20 min). Below pH 4, the equilibrium is shifted toward the monomer at concentrations up to 390 μM. No higher concentration was tested.

Analytical Ultracentrifugation. Due to the slow monomer−dimer equilibration observed in size-exclusion chromatography, we used sedimentation equilibrium to determine the dimer dissociation constant, K_d. The equilibrium distribution was established at rotor speeds of 25 000, 29 000, and 43 000 rpm. Figure 1 shows sedimentation equilibrium data collected at three speeds, with fits to a monomer−dimer self-association model for a protein concentration of 58 μM, and the residuals for the fit. Data from similar experiments at protein concentrations of 19 and 174 μM are shown in Table 1. A global fit of multiple concentrations and speeds gives a dissociation constant of 12 μM and an apparent molecular mass of 17 543 Da (actual molecular mass 20 748 Da). Models incorporating larger oligomeric species were also tested but did not provide acceptable variances. A K_d value of 12 μM determined in PBS buffer, pH 7 and at 4 °C, corresponds to a moderate free energy of dimerization, −6 kcal/mol.

Sedimentation velocity experiments conducted at protein concentrations of 19, 58, and 174 μM (pH 7, 4 °C, PBS buffer) give an average sedimentation velocity coefficient of 1.5 S. The apparent mass corresponding to the best fit diffusion coefficient is 17 kDa, in reasonable agreement with the actual mass of the LC8 dimer.

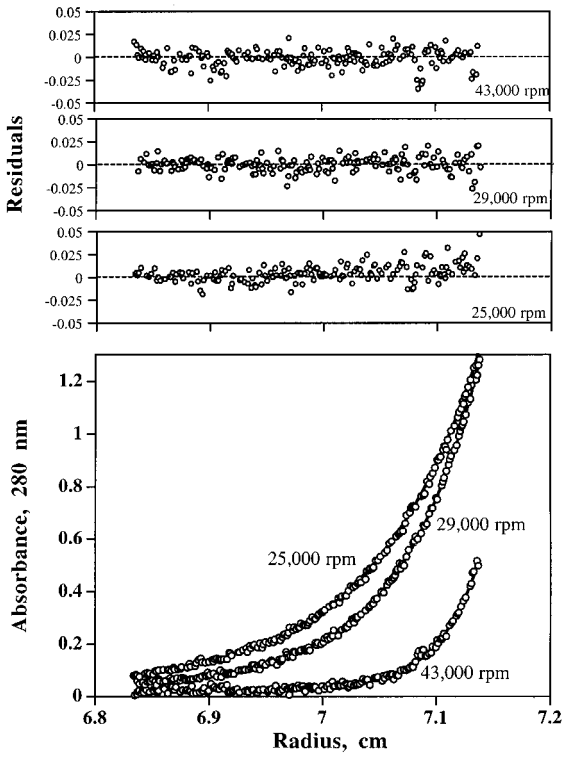

FIGURE 1: Concentration in absorbance units vs radial position profiles for LC8 with a loading concentration of 58 μM at rotor speeds of 25 000, 29 000, and 43 000 rpm. Solutions were in PBS buffer and 10 mM TCEP at pH 7.2 and 4 °C. Equilibrium data were analyzed using a monomer−dimer self-association model. The fitting residuals for each speed are presented in the upper panels. Apparent molecular masses obtained from the model are 18 938 Da (variance 0.76) at 25 000 rpm, 18 701 Da (variance 0.61) for 29 000 rpm, and 16 272 Da (variance 0.86) at 43 000 rpm. Solid lines were simulated by using the parameters obtained from nonlinear least-squares analysis. The global fit of the three speeds gives an apparent molecular weight of 18 604 (variance 0.86). The calculated molecular weight for the dimer is 20 748 Da. Data at 19 and 174 μM show similar parameters and fitting residuals for the same model (Table 1).

Table 1: Sedimentation Equilibrium Data Obtained for LC8 at 4 °C in PBS Buffer, pH 7.2

protein concn (μM)	app mol mass[a] (Da)	variance (Da)
174	17159	4.42
58	18604	0.86
19	17915	1.01

[a] Apparent molecular mass determined from global fit of three speeds, 25 000, 29 000, and 43 000 rpm, to a monomer−dimer self-association model. Data at three concentrations and three speeds for each concentration were globally fit to give an apparent molecular mass of 17 543 Da (variance 2.3 Da) and an association constant of 80 575 M^{-1} (K_d of 12.4 μM).

To determine the effect of lower pH on dimer dissociation, sedimentation equilibrium and velocity measurements were performed on separately prepared samples in the pH range 2.6−8.5. As determined by CD and fluorescence spectroscopy (see below), LC8 has a compact folded structure in this pH range. Table 2 lists the sedimentation velocity coefficients, *s*, and apparent molecular masses obtained from sedimentation equilibrium analysis of three concentrations at three speeds each. A plot of the estimated molecular weight of LC8 obtained from sedimentation equilibrium as a function of pH is shown in Figure 2. In the pH range of

Table 2: Sedimentation Velocity and Equilibrium Data Obtained for LC8 as a Function of pH at 4 °C

pH	mol mass[a] (Da)	s^b	$K_d{}^c$ (μM)
2.5	9287	0.906	
3	9036	0.876	
3.2	9230	–	
3.1#[d]	9125	0.869	
3.5#[d]	9365	0.867	
3.8	9405	–	
4.1	9753	0.949	
5.3#[d]	15387	1.283	42
5.3	15467	1.349	41
7.2	17543	1.52	12
8.5	18287	1.51	6.9

[a] Apparent molecular mass determined from sedimentation equilibrium of three concentrations at three speeds. [b] Sedimentation velocity coefficient determined from sedimentation velocity average of three runs for three concentrations. [c] K_d was determined from global fit to three concentrations and three speeds using the monomer−dimer self-association model. [d] All samples were in 10 mM citrate, phosphate, or Tris buffer containing 0.1 M NaCl, unless indicated by (#). No salt was added to these samples.

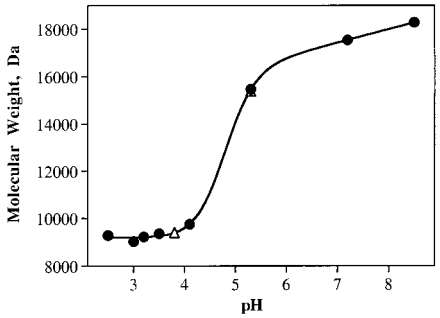

FIGURE 2: Apparent molecular weight of LC8 determined from sedimentation equilibrium experiments as a function of pH. LC8 is a monomer in the pH range of 2−4 and a dimer above pH 5, with a transition midpoint of 4.8. Samples were dialyzed in 10 mM buffer (see Materials and Methods for details), 0.1 M NaCl, and 5 mM TCEP. Data for samples without added salt are shown in open triangles.

2.6−4.0, LC8 is a monomer (at higher pH), and it associates to a dimer with a transition midpoint at pH 4.8. Global analysis of the low pH data with a model that assumes a single species yields a molecular weight corresponding to monomer. Models incorporating dimer in addition to monomer were tested but provided no evidence supporting the presence of larger species in the concentration range of 10−174 μM and pH 2.5−4.5. No detectable difference was found for samples with and without added salt at the same pH (Figure 2).

Circular Dichroism. Changes in structure upon dimer dissociation at low pH were probed by far- and near-UV CD. Far-UV CD monitors changes in secondary structure, and is more sensitive to α-helical conformations. Near-UV CD monitors the local environment of aromatic residues and probes changes in quaternary structure as well as global unfolding. Figure 3 shows spectra of LC8 at pH 7 (dimer) and pH 3 (monomer), at 30 °C and 18 μM protein concentration. Far-UV CD spectra of both LC8 monomer (dashed line) and dimer (solid line) show significant amounts of secondary structure, with little difference between them (Figure 3A). Figure 3B shows near-UV CD spectra dominated by Tyr side chain bands at 276 and 283 nm that are weaker for monomeric LC8 (dashed line). The loss of

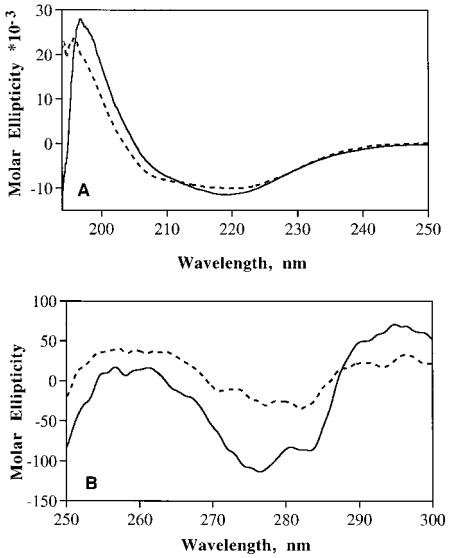

FIGURE 3: Far- (A) and near-UV (B) CD spectra of monomer and dimer LC8. Data were collected on LC8 samples at pH 7 (dimer) and pH 3 (monomer) at a protein concentration of 18 μM. Far-UV CD spectra are similar for monomer (dashed curve) and dimer (solid curve). Near-UV CD spectra show a significant loss of tertiary structure in the monomer (dashed curve), with a major decrease in the negative ellipticity of the Tyr band at 276 nm. Molar ellipticity was calculated assuming a negligible difference between the extinction coefficient of dimer and folded monomer.

intensity in the near-UV spectra, while fluorescence spectra indicate that the monomer is folded, suggests the presence of a Tyr residue at the dimer interface which is perturbed by dissociation to monomer while the tertiary structure is retained.

Fluorescence Emission Spectroscopy. The single tryptophan at position 54 in LC8 makes intrinsic fluorescence an excellent probe to investigate conformational changes in the environment around the fluorophore. Trp fluorescence emission spectra for monomeric and dimeric LC8 show an emission maximum at 327 nm, as commonly observed for buried Trp in a hydrophobic environment in globular proteins (data not shown). There is no detectable difference in the fluorescence emission maximum wavelength between monomer and dimer, indicating that the tertiary structure in the vicinity of Trp 54 is similar in the monomer and dimer. A red shift to a maximum around 350 nm, accompanied by significant loss in intensity, is observed upon unfolding (data not shown).

Stability of Monomeric and Dimeric LC8. The conformational stability of LC8 was estimated from chemical and thermal equilibrium denaturation studies. Figure 4 shows equilibrium unfolding profiles in GdnCl at pH 3 and pH 7, with a protein concentration of 3.5 μM. Fluorescence intensity at 327 nm was measured as a function of increasing concentration of GdnCl. At pH 3, the denaturation profile shows a single transition consistent with the two-state unfolding of a monomer (triangles). Nonlinear least-squares fitting of these data as discussed under Materials and Methods indicates that the free energy of unfolding at pH 3 is 8.0 kcal/mol, the midpoint of unfolding C_m is 3.2 M, and the slope m is -2.5 kcal mol^{-1} M^{-1}. These values are within the range expected for a stable protein with a compact folded core. At pH 7.0 (circles), LC8 is in a monomer−dimer equilibrium, and data are fit to a three-state model (eq 1).

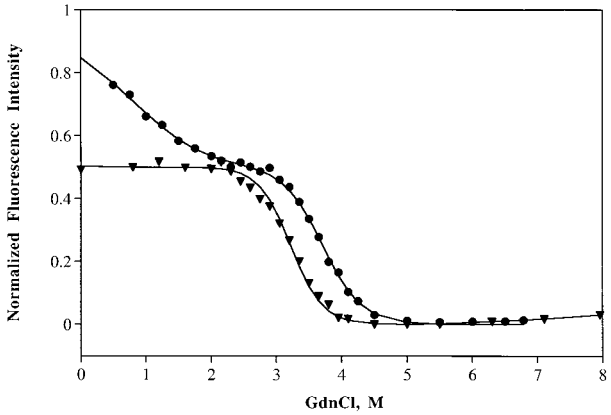

FIGURE 4: GdnCl unfolding profiles of LC8 monomer and dimer as followed by changes in the fluorescence emission intensity at 327 nm. Monomeric LC8 at pH 3 (triangles) and dimeric LC8 at pH 7 (circles) are 3.5 μM in 5 mM TCEP. Data were acquired at 30 °C using a batch-type experiment to ensure that equilibrium was achieved before data acquisition. A reference spectrum was obtained for every GdnCl concentration. Dimer LC8 unfolds by a three-state process with 0.6 and 3.7 M GdnCl midpoints for the first and second transitions, respectively. Monomeric LC8 at pH 3 unfolds with a single transition, midpoint 3.2 M. Solid lines represent nonlinear least-squares fits of the data. The data are normalized so that a population consisting entirely of dimer would have a value of 1, and a completely unfolded sample would have a value of 0. The plateau between the dissociation and unfolding is normalized to 0.5.

Table 3: Thermodynamic Parameters Obtained from Equilibrium Denaturation of LC8 at pH 7

protein concn (μM)	C_{m1}[a] (M)	C_{m2} (M)	m_1 (kcal mol^{-1} M^{-1})	m_2 (kcal mol^{-1} M^{-1})	spectroscopic probe
0.5	(−0.2)	3.8	−2.2	−2.0	fluorescence
0.7	(−0.1)	3.6	−1.7	−2.1	fluorescence
3.5	0.6	3.7	−1.3	−2.0	fluorescence
12.5	0.8	3.7	−2.0	−2.0	near-UV CD
19.4	1.0	3.7	−1.9	−2.0	fluorescence
	−	3.7	−	−2.0	far-UV CD
35	−	3.7	−	−2.0	far-UV CD

[a] These parameters were obtained from a global fit of the data with $\Delta G_{H_2O,1}$ equal to 8.4 kcal/mol and $\Delta G_{H_2O,2}$ equal to 7.5 kcal/mol. See text for explanation.

The midpoint of dimer dissociation, $C_{m,1}$, occurs at 0.6 M, with a ΔG_{H_2O} of 8.4 kcal/mol. The cooperative global unfolding transition has a midpoint at $C_{m,2}$ at 3.7 M, with a ΔG_{H_2O} of 7.5 kcal/mol (Table 3). The complete reversibility of unfolding was confirmed by spectra obtained after the unfolded protein was transferred to a renaturing buffer.

Thermal denaturation monitored by far-UV CD at 222 nm was performed for monomeric LC8 at pH 4.0 and 3.0 μM protein concentration. Monomeric LC8 unfolds with a single transition and a midpoint, T_m, of 64 °C (Figure 5). A similar value for T_m was determined from the loss of fluorescence intensity during thermal unfolding (data not shown). With short exposure to elevated temperature and at low protein concentration, denaturation is about 90% reversible. Prolonged exposure to elevated temperature results in irreversible denaturation. At pH 7.0, thermal denaturation is not reversible (data not shown), and denaturation at a temperature of about 65 °C results in the formation of soluble and insoluble aggregates.

Unfolding of LC8 Dimer. Equilibrium studies of GdnCl-induced denaturation were performed to probe the energetics

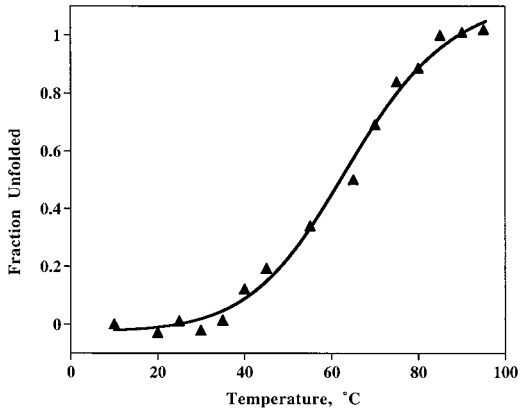

FIGURE 5: Thermal unfolding curve of monomeric LC8 as detected by far-UV CD at 220 nm. The protein sample was at 3 μM concentration and pH 4, 10 mM phosphate buffer, and 2 mM TCEP. Thermal denaturation was 90% reversible with minimal exposure to temperature. Above 65 °C, the temperature was dropped to 25 °C every 5 °C interval and then raised again. Samples were allowed to equilibrate for 5 min at every temperature with continuous stirring. Solid lines represent nonlinear least-squares best fits of the data to a two-state model.

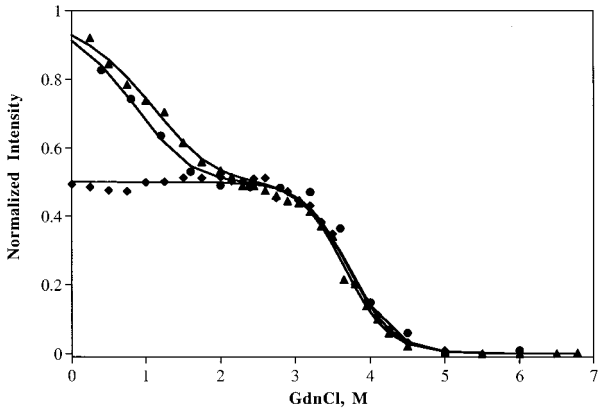

FIGURE 6: GdnCl unfolding profiles monitored by far- and near-UV CD and fluorescence spectroscopy for dimeric LC8 at pH 7. All samples were prepared in 10 mM phosphate, 0.1 M NaCl, and 5 mM TCEP. The protein concentration was 19.4 μM for far-UV CD and fluorescence and 12.5 μM for near-UV CD. Loss of intensity in far-UV CD spectra was monitored at 222 nm (diamonds), and in near-UV CD at 276 nm (circles). Loss of fluorescence intensity was recorded at 327 nm (triangles). Data were acquired at 30 °C as described under Materials and Methods and in the legend to Figure 4. Dimer unfolding is fit to a three-state model (solid lines).

of unfolding of dimeric LC8. Figure 6 shows unfolding profiles of LC8 at pH 7.0 monitored by near-UV CD (circles), fluorescence emission intensity (triangles), and far-UV CD (diamonds). At the sample conditions used for these experiments, LC8 is primarily dimer. The near-UV CD profile shows a pronounced and discrete transition before unfolding, with $C_{m,1}$ = 0.8 M (Table 3). The first transition is characterized by a loss of 35−40% of the signal in near-UV CD and fluorescence, but no loss of the far-UV CD signal at 222 nm. Since the loss of fluorescence intensity is not accompanied by a shift in emission maximum, we conclude that the transition is restricted to quaternary structure, and the product is a monomer which retains native secondary and tertiary structures.

To verify that the first transition is dimer dissociation to folded monomer rather than to a partially folded dimeric

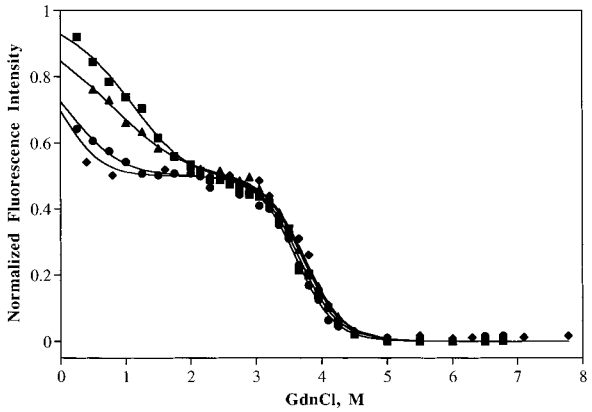

FIGURE 7: Conformational stability of LC8 dimer as a function of protein concentration, as monitored by loss of fluorescence intensity at 327 nm. Protein concentrations in μM are 0.5 (diamonds), 0.7 (circles), 3.5 (triangles), and 19.4 (squares). The midpoints for both transitions are listed in Table 3, together with other data. At a protein concentration of 0.5 μM, the dimer state is not significantly populated. At higher concentrations, a three-state unfolding model best fits the data. All experiments were conducted in 10 mM sodium phosphate, pH 7, 0.1 M NaCl, and 5 mM TCEP.

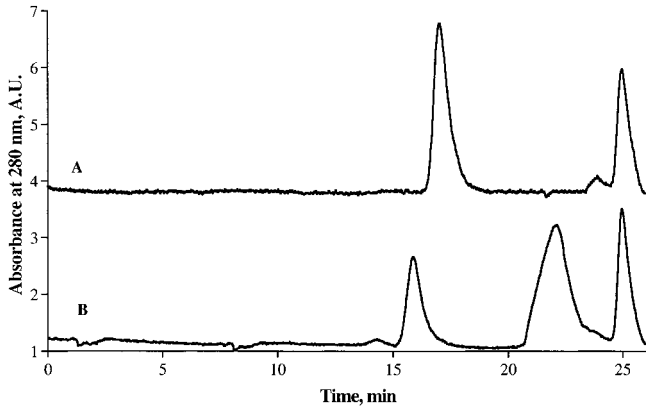

FIGURE 8: Comparison of the association states determined from size-exclusion chromatography of (A) *Drosophila* LC8 and (B) *Aspergilus* LC8 (NudG). Experiments were carried out at flow rate of 1 mL/min. The running buffer used is 0.1 M sodium phosphate, 0.3 M sodium sulfate, 5 mM DTT, pH 7, and elution was monitored by absorbance at 280 nm. Protein concentrations were 35 μM for *Drosophila* LC8 and 50 μM for NudG. NudG shows a high monomer-to-dimer ratio whereas *Drosophila* LC8 is all dimer at this protein concentration and pH. NudG elutes earlier because of its higher molecular mass (monomer mass of 12.1 kDa relative to 10.3 kDa for *Drosophila* LC8). The peak at 25 min is for a small molecule internal standard. The relatively high population of monomer in NudG is possibly explained by the elimination of a hydrogen bond by substitution of Tyr 65 by Phe.

intermediate, we characterized the protein concentration dependence of this change. Table 3 and Figure 7 show the results of GdnCl denaturation of LC8 at pH 7 and 30 °C in the concentration range of 0.5−35 μM as detected by loss of fluorescence intensity at 327 nm. The solid lines of Figure 7 were calculated using a global fit of each data set using eqs 2−8. The best fit was achieved with a free energy of dimer dissociation of 8.4 kcal/mol, and a free energy of unfolding of 7.5 kcal/mol. The data in Figure 7 (and other plots of denaturation curves) were normalized so that a sample which was entirely dimer would have an intensity of 1, a sample which was entirely unfolded monomer would have an intensity of 0, and the plateau between the dissociation and unfolding transitions is at 0.5. The spectroscopic signal associated with dimer LC8 was treated as an adjustable parameter in the model, since under these conditions some monomer is always present and the signal of pure dimer cannot be measured.

As Figure 7 makes clear, dimer dissociation is concentration dependent, and at low protein concentrations, the monomer is the predominant species. The unfolding transition is not concentration dependent, and the midpoint $C_{m,2}$ does not deviate from 3.7 ± 0.1 M over a 70-fold change in protein concentration. The slope of the transition also does not show clear, overall concentration dependence when measured by the same technique, further verifying that reversible monomer unfolding is not affected by concentration in this range. The similarity of unfolding behavior at different concentrations and when monitored by different techniques is strong evidence that unfolding is a simple two-state process.

Comparison to Aspergilus LC8. LC8 from *Aspergilus* (NudG) shares 71% sequence identity with *Drosophila* LC8. Mapping the sequence to the crystal structure of PIN shows that the residues at the dimer interface of PIN are conserved except that in NudG, Tyr 65 is replaced by Phe and Lys 44 is replaced by Arg. We have taken advantage of the fortuitous substitution of residue 65 to investigate whether the interaction between the phenolic OH of Tyr 65 and Lys 44 Nϵ contributes to the stability of the dimer. Figure 8 shows analytical size-exclusion chromatograms of *Drosophila* LC8 (A) and of NudG (B) at pH 7 and identical buffer conditions. Two peaks are observed for NudG, a dimer peak at 16 min and a monomer peak at 22 min, and the monomer is predominant over the dimer. In contrast, for *Drosophila* LC8 (A), no monomer peak is detected, indicating that *Drosophila* LC8 is a tight dimer at this pH. The relative abundance of monomer NudG suggests that Tyr 65 is involved in a stabilizing H-bond across the dimer interface of LC8. This conclusion is based on the assumption that the unconserved residues of NudG that are not at the PIN dimer interface do not have a role in dimer stability.

DISCUSSION

LC8 Is a Dimer at Physiological pH. Drosophila LC8 is a moderately tight dimer at pH 7 with a dissociation free energy change of 6 kcal/mol (K_d of 12 μM) as determined from sedimentation equilibrium studies at 4 °C, and 8.4 kcal/mol as determined from GdnCl denaturation at 30 °C. In the following discussion, we will be comparing this result with previous structural studies of LC8, which have typically used mammalian LC8 (PIN). Since the primary sequence of PIN is 94% identical to *Drosophila* LC8, and the remaining 6% are of the same charge, the two variants are expected to show similar association behavior.

PIN has previously been reported to be a dimer at pH 7.5, with no observable monomer or higher aggregate, based on gel filtration experiments (*15*). More recent gel filtration experiments have been reported which indicate that PIN is a slowly interconverting monomer−dimer equilibrium at pH 8, and fully dimeric at pH 5.5 (*21*). PIN was also reported to be a monomer at pH 6 based on an NMR structure (*22*), but later work from the same lab using analytical ultracentrifugation indicated that PIN is a trimer at protein concentrations of 0.03 mM and higher (*23*).

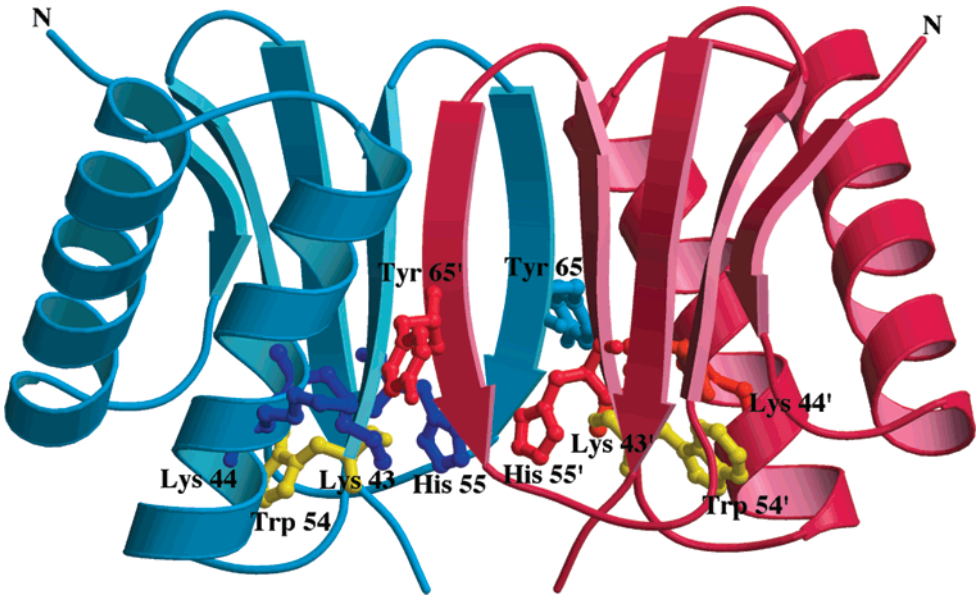

FIGURE 9: Ribbon diagram of PIN dimer, with monomeric subunits colored in red and blue. Residues from each subunit important for stabilization of the dimer interface are shown in ball-and-stick drawing in shades of blue and red for each subunit. The dimer-stabilizing residues highlighted here are the hydrogen bond (N−O distance 2.8 Å) between the side chains of Tyr 65 and Lys 44′ and the close-packed (5.7 Å separation) histidine rings 55 and 55′. Lys 43 Nϵ is 5.7 Å distant from His 55 of the same chain, and protonation of His 55 at low pH would cause dimer-destabilizing repulsive interactions. Trp 54 of both subunits is shown in yellow and is buried in the core of each monomer. The structure of PIN bound to a 13-residue peptide was solved by X-ray diffraction (*21*). The peptide is not shown in this drawing. PIN image was produced using Molscript (*39*) and rendered by Raster3d (*40*).

The discrepancies between our work and previous reports may be due in part to the slow monomer−dimer equilibration of LC8. In our sedimentation equilibrium experiments, we ascertained that equilibrium was attained by confirming that sequential scans at the same conditions were identical. We also used high rotor speeds, which are necessary for proteins of this size to ensure that a gradient is formed. The results of independent measurements at three protein concentrations were both individually and globally fit, with random residuals, to a monomer−dimer model (Figure 1 and Table 1). This result indicates that there is no systematic deviation from the monomer−dimer model, and that there are no soluble higher aggregates at high concentration. Other models that incorporated monomer or trimer species produced variances well out of the accepted range.

The physiological concentration of LC8 is very likely in the sub-micromolar range, and at these concentrations our work shows that LC8 is predominantly monomeric in vitro. However, it is reasonable to expect that LC8 is a dimer in vivo since self-association is significantly enhanced in crowded fluids such as the cytoplasm (*33*). Furthermore, covalent cross-linking experiments on purified samples of brain cytoplasmic dynein, myosin V, and *Chlamydomonas* dynein show that LC8 is a homodimer in situ (*20*).

Dimerization Is pH-Dependent. We determined the full pH and protein concentration profile of *Drosophila* LC8 association states by sedimentation equilibrium and velocity techniques. *Drosophila* LC8 is a dimer at pH 7 and is completely dissociated to monomer below pH 4 (Figure 2 and Table 2). To explain this titration behavior, we have examined the crystal structure of PIN homodimer with a bound peptide fragment of nNOS (*21*). The dimer interface of PIN is primarily hydrophobic. Hydrophobic contacts across the interface which could stabilize the dimer at neutral pH include Ile 57/57′, Phe 62/62′, and Phe 86/86′. Another feature of the dimer interface is the ring stacking of His 55 and His 55′. In addition, there are six O−N distances of less than 3.0 Å across the interface, indicative of intermolecular hydrogen bonds between side chains of Lys 43 and Thr 67′, side chains of Lys 44 and Tyr 65′, and backbones of Val 58 and Gly 63′.

The pH-dependent dissociation of LC8 implies pH titration of one or more critical groups. In general, protonation may cause dimer dissociation by eliminating a favorable charge/charge interaction between residues, or by introducing an unfavorable interaction between like charges. The pH titration effect on dimerization most likely takes place within the dimer interface, although effects of a distant residue cannot be ruled out a priori. Of the residues at the interface of LC8 which could titrate between pH 4 and 5, His 55 and 55′ are the most probable candidates. Since they are separated by less than 6 Å, protonation of these residues would create a repulsive interaction buried in the dimer interface. In addition, protonation of His 55 could also lead to repulsive interaction with the positively charged Lys 43 side chain, which is less than 6 Å distant on the same subunit (Figure 9). If protonation of His 55 is primarily responsible for pH-dependent dimer dissociation, the pK_a of His 55 would be about 4.8 (Figure 2). This deviation from the normal pK_a of 6.0 is expected for an imidazole group buried in a hydrophobic environment and in proximity to positively charged lysine residues. Point mutations of His 55 and other residues at the dimer interface of *Drosophila* LC8 are currently in progress in our lab to further test the hypothesis that titration of His 55 is the primary cause of dissociation at low pH.

At neutral pH, the interactions that stabilize the dimer appear to be hydrophobic contacts and intermolecular H-bonds as mentioned above. One of these H-bonds is missing in a variant of LC8 from *Aspergilus* (NudG), which has Phe

in place of Tyr 65, while all other residues in the interface are of the same polarity. The hydrogen bonding partner of Tyr 65, Lys 44, is replaced by Arg. NudG is a far weaker dimer than *Drosophila* LC8, and dissociates to a monomer at higher protein concentrations and milder conditions (Figure 8). Weaker interaction between the subunits of the NudG dimer is most simply explained by a reduction in the number of possible hydrogen bonding interactions. The involvement of Tyr 65 in important interactions in stabilizing the dimer interface is also consistent with our observation that the near-UV CD signal at 276 nm, which is sensitive to tyrosine environment, is significantly less intense for monomer compared to dimer (Figure 3B).

Monomeric LC8 Is Compact and Stable. Far-UV CD spectra of dimer LC8 and pH-dissociated monomer LC8 are similar, indicating that there is no detectable loss in secondary structure associated with dissociation (Figure 3A). Fluorescence emission spectra are also similar for dimer and monomer, with no red shift in the fluorescence emission wavelength maximum, suggesting that the unique Trp 54 residue is still buried in the core of the monomer after dissociation (Figure 9). A diminished near-UV CD signal at 276 nm upon dissociation is due to loss of quaternary structure, and not loss of tertiary structure (Figure 3B). The near-UV CD signal arises primarily from Tyr 65, and the change in intensity is evidence that its local environment is altered significantly in the monomer compared to the dimer. (Near-UV CD spectra of NudG, an LC8 variant in which Tyr 65 is substituted by Phe, lack the signal at 276 nm, supporting the conclusion that in *Drosophila* LC8 this band arises from Tyr 65.) Complete loss of signal is observed upon denaturation.

The monomeric state of LC8 is also populated at low protein concentration with no GdnCl, and in 1−2.5 M GdnCl of more concentrated samples at pH 7 (Figure 7). Both the pH-dissociated monomer and the monomer at low protein concentrations retain native tertiary structure and undergo cooperative, reversible unfolding. They are of comparable stability, with a free energy change for unfolding of 8.0 and 7.5 kcal/mol, respectively. Identifying conditions at which either monomer or dimer predominates and is amenable to solution studies is essential for addressing fundamental questions about macromolecular complexes such as binding sites, conformational changes, and forces that drive assembly.

Folding and Assembly of the LC8 Dimer. Equilibrium denaturation studies were used to probe the sequence of events in dimer unfolding, and the energetics of each step. GdnCl unfolding profiles of dimeric LC8 show two distinct transitions. Both near-UV CD and fluorescence indicate that the first transition is concentration dependent, with a free energy (ΔG_{H_2O}) of 8.4 kcal/mol at pH 7.0. The free energy of the second transition is 7.5 kcal/mol, and its midpoint is concentration independent, occurring at 3.7 M over a broad range of protein concentrations (Table 3). These observations are best explained by a three-state model (eq 1) in which the dimer dissociates in a second-order process to a fully folded monomeric intermediate followed by first-order unfolding. A similar dimer denaturation pathway has been observed for Cu, Zn superoxide dismutase (*34*) and human interleukin 10 (*35*) among other examples. In the case of human interleukin 10, dissociation occurs at 1.6 M GdnCl or pH 2.5, similar to our work. In contrast, several dimeric proteins unfold with no stable intermediate, for example, arc repressor and beta-nerve growth factor (*32*, *36*), while other dimers unfold with a partially folded monomeric or dimeric intermediate (*37*, *38*). We suggest that the sequence of events for LC8 dimer formation starts with independent folding of monomer subunits before assembly into an active dimer, which may then be followed by the assembly of the other subunits into the functional dynein complex.

The moderate intersubunit binding and a stable monomeric form of LC8 suggest a functional role for monomeric LC8, and this may partially explain the multiple interactions involving LC8 that have been reported. In the crystal structure of PIN bound to a 13-residue peptide from nNOS, the peptide binding site is adjacent to the dimer interface, and although each peptide is clearly associated more closely with one of the monomers, there are close contacts with both chains of the homodimer. The structure suggests that cargo may bind to monomer or dimer under varying conditions. The involvement of a functional monomer in the multiplicity of interactions of LC8 with other proteins could provide an evolutionary constraint against mutations that destabilize the monomer, and account for the high conservation of the LC8 subunit between different organisms. It will be important in future studies to demonstrate both in vitro and in vivo the functional significance of monomer interactions, and to explore the potential role of LC8 dimerization in the activation of complex assembly and cargo binding.

CONCLUSIONS

We have characterized the monomer−dimer equilibrium, determined monomer and dimer stability, and identified residues that likely contribute to dimer formation of LC8, a highly conserved dynein light chain. Equilibrium denaturation, sedimentation equilibrium, and sedimentation velocity all show that LC8 is a moderately tight dimer at physiological pH. At very low protein concentration ($<0.5\ \mu$M), in 1−2.5 M GdnCl, or below pH 4.8, LC8 dissociates to a stable monomer that retains native secondary and tertiary structures. Dissociation of the dimer at low pH is best explained by protonation of His 55/55′ at the dimer interface, which introduces a repulsive interaction and incurs the energetic penalty of burying two positive charges. Studies on NudG, a variant of LC8 lacking Tyr 65 which is primarily monomer under conditions where LC8 is a dimer, support the proposal that a hydrogen bond between Tyr 65 and Lys 44′ is important for LC8 dimer stability. The formation of a folded, stable monomer suggests a role for monomer−dimer equilibrium in LC8 function, and may explain the multiple roles that LC8 plays in dynein assembly and binding to cargo. The spectroscopic probes for secondary, tertiary, and quaternary structural features which we have identified will facilitate ongoing studies of the influence of the association state of LC8 on its interactions with other subunits of dynein and with cargo.

ACKNOWLEDGMENT

We thank Dr. J. Lee and Dr. C. Chen at The University of Texas Medical Branch at Galveston for performing the analytical ultracentrifugation studies. We also thank Dr. B. Liu at the University of California, Davis, for the *Aspergilus*

LC8 plasmid, and Dr. J. Clardy at Cornell University for providing coordinates of the PIN dimer.

REFERENCES

1. Vallee, R. B., and Sheetz, M. P. (1996) *Science 271*, 1539−1544.
2. Harada, A., Takei, Y., Kanai, Y., Tanaka, Y., Nonaka, S., and Hirokawa, N. (1998) *J. Cell Biol. 141*, 51−59.
3. King, S. M. (2000) *Biochim. Biophys. Acta 1496*, 60−75.
4. Pfister, K. K., Salata, M. W., Dillman, J. F., Torre, E., and Lye, R. J. (1996) *Mol. Biol. Cell 7*, 331−343.
5. Dick, T., Surana, U., and Chia, W. (1996) *Mol. Gen. Genet. 251*, 38−43.
6. Dick, T., Ray, K., Salz, H. K., and Chia, W. (1996) *Mol. Cell. Biol. 16*, 1966−1977.
7. Hoffmann, K. F., and Strand, M. (1996) *J. Biol. Chem. 271*, 26117−26123.
8. Beckwith, S. M., Roghi, C. H., Liu, B., and Morris, N. R. (1998) *J. Cell Biol. 143*, 1239−1247.
9. King, S. M., and Patel, K. R. (1995) *J. Biol. Chem. 270*, 11445−11452.
10. Phillis, R., Statton, D., Caruccio, P., and Murphey, R. K. (1996) *Development 122*, 2955−2963.
11. Pazour, G. J., Wilkerson, C. G., and Witman, G. B. (1998) *J. Cell Biol. 141*, 979.
12. King, S. M., Barbarese, E., Dillman, J. F., Benashski, S. E., Do, K. T., Patel-King, R. S., and Pfister, K. K. (1998) *Biochemistry 37*, 15033−15041.
13. Espindola, F. S., Cheney, R. E., King, S. M., Suter, D. M., and Mooseker, M. S. (1996) *Mol. Biol. Cell 7*, 2160−2160.
14. Jaffrey, S. R., and Snyder, S. H. (1996) *Science 274*, 774.
15. Rodriguez-Crespo, I., Straub, W., Gavilanes, F., and de Montellano, P. R. O. (1998) *Arch. Biochem. Biophys. 359*, 297−304.
16. Crepieux, P., Kwon, H., Leclerc, N., Spencer, W., Richard, S., Lin, R. T., and Hiscott, J. (1997) *Mol. Cell. Biol. 17*, 7375.
17. Puthalakath, H., Huang, D. C. S., O'Reilly, L. A., King, S. M., and Strasser, A. (1999) *Mol. Cells 3*, 287−296.
18. Schnorrer, F., Bohmann, K., and Nusslein-Volhard, C. (2000) *Nat. Cell Biol. 2*, 185−190.
19. Epstein, E., Sela-Brown, A., Ringel, I., Kilav, R., King, S. M., Benashski, S. E., Yisraeli, J. K., Silver, J., and Naveh-Many, T. (2000) *J. Clin. Invest. 105*, 505−512.
20. Benashski, S. E., Harrison, A., Patel-King, R. S., and King, S. M. (1997) *J. Biol. Chem. 272*, 20929−20935.
21. Liang, J., Jaffrey, S. R., Guo, W., Snyder, S. H., and Clardy, J. (1999) *Nat. Struct. Biol. 6*, 735−740.
22. Tochio, H., Ohki, S., Zhang, Q., Li, M., and Zhang, M. J. (1998) *Nat. Struct. Biol. 5*, 965−969.
23. Fan, J. S., Zhang, Q. A., Li, M., Tochio, H., Yamazaki, T., Shimizu, M., and Zhang, M. J. (1998) *J. Biol. Chem. 273*, 33472−33481.
24. Pace, C. N., and Scholtz, J. M. (1997) in *Protein Structure: A Practical Approach* (Creighton, T. E., Ed.) pp 299−322, Oxford University Press, Oxford.
25. Pace, C. N., Vajdos, F., Fee, L., Grimsley, G., and Gray, T. (1995) *Protein Sci. 4*, 2411−2423.
26. Ellman, G. L. (1959) *Arch. Biochem. Biophys. 82*, 70−77.
27. Guan, K. L., and Dixon, J. E. (1991) *Anal. Biochem. 192*, 262−267.
28. Cheng, X. D., Gonzalez, M. L., and Lee, J. C. (1993) *Biochemistry 32*, 8130−8139.
29. Santoro, M. M., and Bolen, D. W. (1988) *Biochemistry 27*, 8063−8068.
30. Neet, K. E., and Timm, D. E. (1994) *Protein Sci. 3*, 2167−2174.
31. Noland, B. W., Dangott, L. J., and Baldwin, T. O. (1999) *Biochemistry 38*, 16136−16145.
32. Bowie, J. U., and Sauer, R. T. (1989) *Biochemistry 28*, 7139−7143.
33. Minton, A. P. (2000) *Curr. Opin. Struct. Biol. 10*, 34−39.
34. Malvezzi-Campeggi, F., Stroppolo, M. E., Mei, G., Rosato, N., and Desideri, A. (1999) *Arch. Biochem. Biophys. 370*, 201−207.
35. Syto, R., Murgolo, N. J., Braswell, E. H., Mui, P., Huang, E., and Windsor, W. T. (1998) *Biochemistry 37*, 16943−16951.
36. Timm, D. E., and Neet, K. E. (1992) *Protein Sci. 1*, 236−244.
37. Gloss, L. M., and Matthews, C. R. (1997) *Biochemistry 36*, 5612.
38. Kasimova, M. R., Milstein, S. J., and Freire, E. (1998) *J. Mol. Biol. 277*, 409.
39. Kraulis, P. J. (1991) *J. Appl. Crystallogr. 24*, 946−950.
40. Merritt, E. A., and Bacon, D. J. (1997) *Methods Enzymol. 277*, 505−524.

BI002278+